Dynamic Stiffness and Damping of a Shallow Foundation from Forced Vibration of a Field Test Structure

Salih Tileylioglu, A.M.ASCE[1]; Jonathan P. Stewart, F.ASCE[2]; and Robert L. Nigbor, M.ASCE[3]

Abstract: Foundation impedance ordinates are identified from forced vibration tests conducted on a large-scale model test structure in Garner Valley, California. The structure is a steel moment frame with removable cross-bracing, a reinforced concrete roof, and a nonembedded square slab resting on Holocene silty sands. Low-amplitude vibration is applied across the frequency range of 5–15 Hz with a uniaxial shaker mounted on the roof slab. We describe procedures for calculating frequency-dependent foundation stiffness and damping for horizontal translational and rotational vibration modes. We apply the procedures to test data obtained with the structure in its braced and unbraced configurations. Experimental stiffness ordinates exhibit negligible frequency dependence in translation but significant reductions with frequency in rotation. Damping increases strongly with frequency, is stronger in translation than in rocking, and demonstrates contributions from both radiation and hysteretic sources. The impedance ordinates are generally consistent with numerical models for a surface foundation on a half-space, providing that soil moduli are modestly increased from free-field values to account for structural weight, and hysteretic soil damping is considered. **DOI: 10.1061/(ASCE)GT.1943-5606.0000430.**

CE Database subject headings: Seismic effects; Soil-structure interactions; Shallow foundations; In situ tests; Vibration.

Author keywords: Seismic soil-structure interaction; Shallow foundations; In situ testing.

Introduction

Impedance functions represent the frequency-dependent stiffness and damping characteristics of foundation-soil interaction. A synthesis of available numerical solutions for impedance functions is given by Gazetas (1991). Those solutions generally utilize assumptions of foundation rigidity and uniform soil of infinite depth with a fixed hysteretic damping ratio. Under these conditions, the soil profile is referred to as a viscoelastic half-space. Additional formulations are available to account for a specified depth-variable shear stiffness (Gazetas 1991; Vrettos 1999), foundation embedment (e.g., Apsel and Luco 1987), and nonrigid foundations (e.g., Iguchi and Luco 1982). This paper is concerned with the experimental evaluation of impedance functions with forced vibration testing of structures in the field. Experimental verification of numerical impedance function solutions is essential to understanding their reliability and applicability to relatively complex field conditions.

In the following two sections, we review the mathematical definition of impedance functions and summarize previous experimental investigations of frequency-dependent foundation stiffness and damping, which places the contribution of the present work in context. We then describe forced vibration tests carried out on a large-scale model test structure in Garner Valley, California, and the evaluation of impedance ordinates from the data. The Garner Valley structure is unique in that it can be configured at two distinct levels of structural stiffness—effectively enabling the evaluation of impedance ordinates for two different structures resting on the same soil profile. Testing is performed at low force levels so the structure and soil remain in the elastic range. We conclude by comparing the experimental results with the predictions of numerical models and by discussing the misfits that are identified.

Theoretical Model for Impedance of a Rectangular Foundation

Impedance functions represent the stiffness and damping characteristics of foundation-soil interaction under cyclic loads. For example, classical solutions for the complex-valued impedance function (Veletsos and Wei 1971; Gazetas 1991) can be written as

$$\bar{k}_j = k_j + i\omega c_j \tag{1a}$$

where $\bar{k}_j$ = complex-valued impedance function; subscript j = index denoting modes of translational displacement or rotation; k_j and c_j = foundation stiffness and damping, respectively, for mode j; and ω = angular frequency (rad/s). An alternative form for Eq. (1*a*) is

$$\bar{k}_j = k_j(1 + 2i\beta_j) \tag{1b}$$

where

$$\beta_j = \frac{\omega c_j}{2k_j} \tag{2}$$

An advantage of using β_j over c_j is that at resonance of the soil-foundation-structure system, the former is interpreted as a percentage of critical damping in the classical sense (Clough and Penzien 1993).

For a rigid rectangular foundation [geometry depicted in Fig. 1(a)] resting on the surface of a half-space with shear wave velocity V_s, Pais and Kausel (1988) review impedance solutions

[1]Senior Staff Engineer, Ninyo and Moore, 475 Goddard, Irvine, CA 92618; formerly, graduate student, Dept. of Civil and Environmental Engineering, UCLA (corresponding author). E-mail: salih@uclalumni.net

[2]Professor and Vice Chair, Dept. of Civil and Environmental Engineering, UCLA, 5731 Boelter Hall, Los Angeles, CA 90095.

[3]Research Engineer, Dept. of Civil and Environmental Engineering, UCLA, 5731 Boelter Hall, Los Angeles, CA 90095.

Note. This manuscript was submitted on October 2, 2009; approved on October 7, 2010; published online on August 18, 2010. Discussion period open until September 1, 2011; separate discussions must be submitted for individual papers. This paper is part of the ***Journal of Geotechnical and Geoenvironmental Engineering***, Vol. 137, No. 4, April 1, 2011. ©ASCE, ISSN 1090-0241/2011/4-344–353/$25.00.

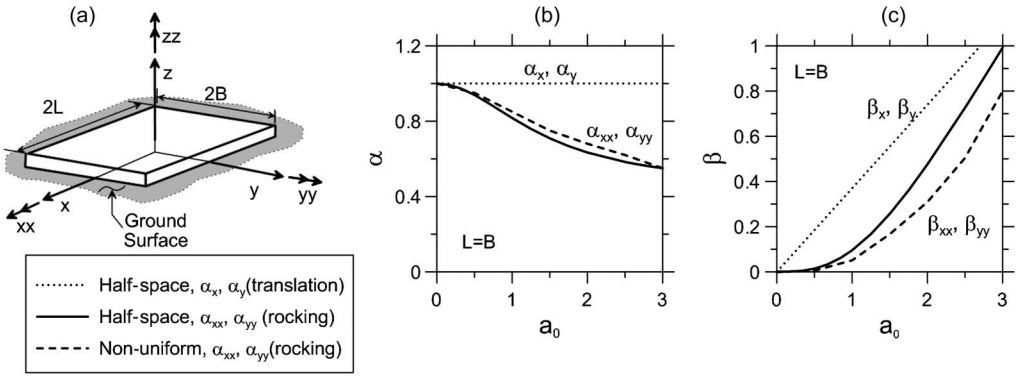

Fig. 1. (a) Geometry of rectangular foundation used in impedance models; (b) and (c) dynamic modifiers for impedance functions of square foundation [adapted from Pais and Kausel (1988) and Vrettos (1999)]; the Vrettos solutions are for a shear modulus profile that doubles from depth zero to depth infinity

in the literature and present fitting equations for the stiffness and damping terms from Eq. (1*a*). Referring to Fig. 1(a), the solutions describe translational stiffness along axes x, y, and z, and stiffness against rotation around those axes (denoted xx, yy, and zz). Damping solutions are also provided. Stiffness k_j is proportional to the static foundation stiffness for mode j, denoted K_j, which in turn depends on soil shear modulus G, foundation dimensions, and soil Poisson's ratio (ν)

$$k_j = K_j \times \alpha_j \tag{3a}$$

where

$$K_j = GB^m f(B/L, \nu), \quad \alpha_j = \alpha_j(B/L, a_0) \tag{3b}$$

and $m = 1$ for translation and $m = 3$ for rotation. The α_j terms are dynamic modifiers of the static stiffness depending on dimensionless frequency a_0

$$a_0 = \frac{\omega B}{V_s} \tag{4}$$

Fig. 1(b) shows analytical solutions for stiffness dynamic modifiers (α terms) whereas Fig. 1(c) shows damping dynamic modifiers (β terms) neglecting the hysteretic component. Solutions are shown both for a uniform half-space (by using the approximate formulas of Pais and Kausel 1988) and a nonuniform media (Vrettos 1999).

For translational modes, stiffness modifiers (α_x, α_y) are nearly frequency-independent, indicating that the real part of the translational impedance function [Eq. (1*a*)] is also frequency-independent. Damping terms for translation (β_x, β_y) increase linearly with frequency. Rotational modes show more frequency-dependent stiffness modifiers and nonlinear variations of damping with frequency. Fig. 1(b) shows that rotational stiffness terms are not significantly affected by soil nonuniformity, whereas Fig. 1(c) shows that damping is reduced.

It is common in engineering practice to neglect the α_j terms (ASCE 2006) and to indirectly account for dashpots c_j by using a foundation system viscous damping ratio β_f (BSSC 2009; ASCE 2006). Hence, ASCE (2006) guidelines provide equations for static stiffness (which are adapted from Pais and Kausel 1988) but do not discuss dashpots or dynamic modifiers for stiffness. The rationale for ignoring dynamic stiffness modifiers is because they are close to 1 for the low frequencies typically of interest for building structures, although this has been questioned for rotational stiffness (Stewart et al. 2003). In this paper, we examine the full, frequency-dependent foundation stiffness (and damping), which provides insight into the degree to which this common simplifying assumption is reasonable for realistic field conditions.

Previous Experimental Evaluations of Impedance Ordinates

Experimental investigations of impedance functions typically seek to evaluate stiffness and damping terms for horizontal translation ($j = x$ or y) and rotation within the vertical plane ($j = xx$ or yy). Cyclic excitation is generally provided by a shaker installed on the roof or foundation of a structure. The first field investigations of foundation impedance provided results over a limited range of frequencies (Lin and Jennings 1984; Luco et al. 1988; Wong et al. 1988) or for small structures representative of strong motion instrument huts (Crouse et al. 1990). More recently, de Barros and Luco (1995) tested the relatively large model structure of a nuclear reactor and provided impedance ordinates over a relatively wide frequency range (~4–20 Hz). Fig. 2 shows impedance ordinates evaluated by de Barros and Luco; the results, which are shown in nonnormalized form because of the uncertain shear modulus of the foundation soils, illustrate the noisy character of the data, especially at frequencies under 4 or greater than 14 Hz. Also shown in Fig. 2 are three model predictions for stiffness and damping, which result from uncertainty in the appropriate V_s value to use with numerical solutions.

Laboratory-scale investigations of foundation-soil interaction were also performed (Richart and Whitman 1967; Dobry et al. 1986; Nii 1987; Gazetas and Stokoe 1991; Gadre and Dobry 1998; Gajan and Kutter 2008). These tests provide valuable insights, especially under conditions involving highly nonlinear soil behavior. However, laboratory tests are limited in their ability to reproduce certain field conditions (Novak 1987). For example, the finite size of the laboratory test container precludes radiation damping of waves with quarter-wavelengths on the order of the container dimension [as reported by Dobry et al. 1986, Fig. 6(a)]. For this reason we emphasize field testing, which involves realistic boundary conditions essential for model calibration.

Two practical difficulties associated with field testing for impedance ordinates and comparison to model predictions have been encountered in previous work. First, limited resolution of the data acquisition system with respect to analog-to-digital signal conversion and time-stamping contribute significant noise to the results. Most previous studies have not formally evaluated noise effects, which can lead to spurious results (e.g., impedance ordinates in Fig. 2 for frequencies outside the 4–14 Hz range). A more complete

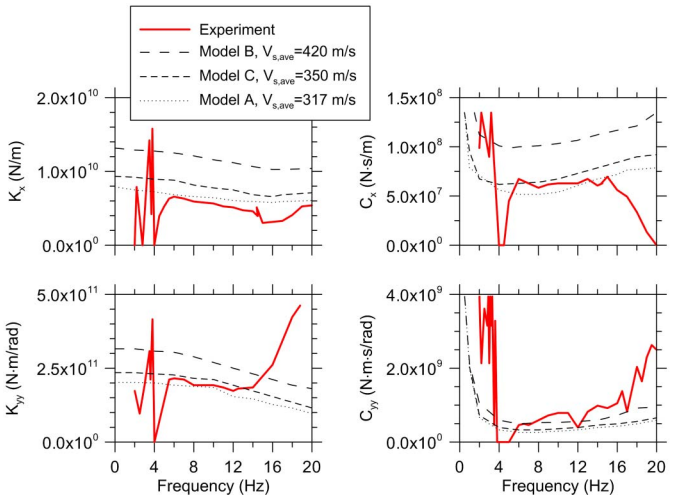

Fig. 2. Translational (top) and rotational (bottom) impedance values for the model of a nuclear containment structure at Hualien, Taiwan (adapted from de Barros and Luco 1995)

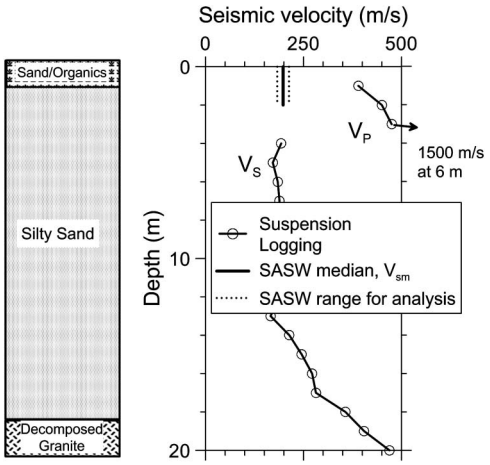

Fig. 3. Soil profile with shear wave velocities obtained from suspension logging and SASW tests [J. Steidl, personal communication 2009; SASW data from Stokoe et al. (2004)]

discussion of these problems is presented in Stewart et al. (2005). Second, shear wave velocity profiles have generally been established with downhole or suspension logging methods in the free-field. This presents two problems. First, those geophysical methods have limited resolution very near the ground surface (e.g., Andrus et al. 2004). Because the soil materials immediately below the foundation exert the greatest influence on foundation stiffness, this introduces uncertainty to the selection of a V_s value for use with numerical solutions. Second, seismic velocities measured in the free-field neglect the effect of confinement provided by the weight of the structure.

The available inventory of test data on impedance ordinates is limited and does not always favorably compare to numerical models. Given the increasingly common use of foundation modeling in performance-based seismic design (ASCE 2006), the lack of data against which to verify numerical model predictions is a concern. This paper presents (1) a methodology for data interpretation to evaluate foundation impedance functions; and (2) a data set obtained by using high-fidelity modern sensors and data acquisition equipment, which provides relatively high signal-to-noise ratios and robust time-stamping. The effects of noise on the results are evaluated to establish the usable frequency range of the experimental ordinates. Moreover, velocity profiling is configured to examine near-surface and deeper features so numerical models are exercised with greater confidence.

Site and Structure Description

The model test structure is located in a sedimentary basin instrumented as part of the Garner Valley Differential Array (GVDA), which in turn is part of the George E. Brown Jr. Network for Earthquake Engineering Simulation (NEES). As shown in Fig. 3, soil conditions consist principally of silty sand materials extending to a depth of 18 m, which are underlain by decomposed granite. Relatively intact crystalline bedrock occurs at a depth of 88 m. The groundwater table is at the surface in rainy seasons and drops to approximately 3 m in dry seasons. Geophysical tests [suspension logging and spectral analysis of surface waves (SASW)] were carried out to measure S-wave velocities with results shown in Fig. 3. Three SASW arrays were positioned on the ground immediately adjacent to the structure (Stokoe et al. 2004). Two dispersion curves were obtained with frequency-independent phase velocities over a wavelength range of 0.6–6.0 m. Those phase velocities have a central value (median) of 198 m/s and a relatively narrow range of ± approximately 15 m/s. The third dispersion curve has more scatter and a lower median phase velocity for wavelengths under 4 m of approximately 170 m/s. Averaging the three medians and correcting phase velocities to shear wave velocities provides an estimated median of $V_{sm} = 198$ m/s. The range for subsequent analysis is taken as 183–213 m/s, which is somewhat narrower than $V_{sm}\pm$ the standard deviation of converted phase velocities (σ_v) owing to the wide scatter in the third array. Additional free-field measurements at the site indicated velocities as low as 120–170 m/s in the upper 6 m—the relatively fast velocities near the structure are likely attributable, at least in part, to the overburden provided by the test structure. The mass density is taken as 1,800 kg/m^3 and Poisson's ratio as 0.35.

The test structure was constructed specifically to facilitate soil-structure interaction (SSI) experiments and hence is referred to as the NEES soil-foundation-structure interaction (SFSI) test structure. As shown in Fig. 4, the structure consists of a simple steel frame supporting a roof slab 40.6 cm in thickness. The foundation consists of a nonembedded reinforced concrete slab 50.8 cm thick. The height of the structure from base of the foundation to the top of roof slab is 4.56 m. The plan dimensions of the foundation and roof slabs are 4.06 m × 4.06 m. Reconfigurable bracings are inserted into the structure to modify its vibration characteristics. The mass of the foundation and roof slab are 20.5 and 16.4 Mg, respectively, on the basis of an assumed concrete unit weight of 23.9 kN/m^3 (152 lb/ft^3). The masses of the intermediate structural elements are 1.7 and 2.0 Mg for the unbraced and braced configurations, respectively. The SFSI test structure is instrumented with triaxial and uniaxial accelerometers, shown in Fig. 4, and other sensors not used in the present research but described by Youd et al. (2004). Signals are digitally recorded at 24-bit resolution and a 200 Hz sample rate. Forced vibration is applied with a uniaxial shaker mounted on the bottom of the top slab (Acoustic Power Systems' Model 113 shaker with dynamic mass = 35.65 kg).

In addition to forced vibration tests, many small earthquakes have been recorded at the Garner Valley test site. Tileylioglu (2008) used both data sets to identify the flexible and fixed-base fundamental mode frequencies listed in Table 1. The fixed-base properties represent the structure alone (no effect of foundation

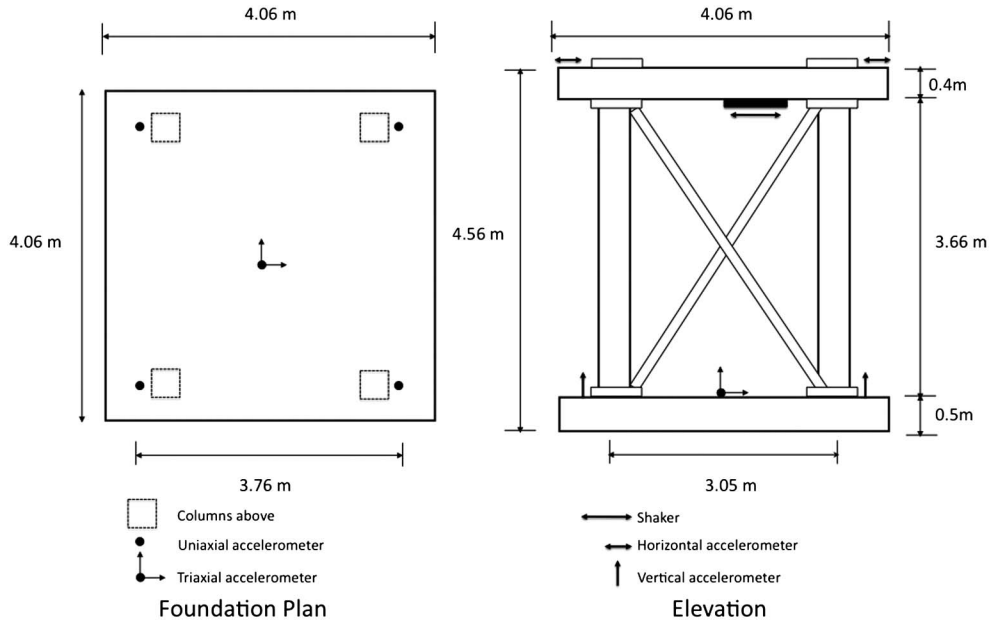

Fig. 4. Plan and elevation views of the SFSI test structure at GVDA showing locations of instrumentation and shaker

compliance or damping) whereas the flexible-base properties represent the complete system.

Derivation of Impedance Functions from Forced Vibration Tests

In this section, equations are derived for the calculation of impedance functions from acceleration recordings at the roof (translation) and base-level (translation, rotation from two vertical instruments) of the structural system. The model representing the soil-foundation-structure system is depicted in Fig. 5, and has one above-ground structural degree of freedom in translation. The rotational degree of freedom of the top slab is neglected by this procedure, but has a negligible effect in the frequency range used in the tests (5–15 Hz). The compliance of the soil is modeled through springs that enable foundation translation (u_f) and rotation (θ_f) relative to the free-field. Deformation of the structural degree of freedom relative to the translated and rotated foundation is denoted u_s.

The equations of motion for the model in Fig. 5 subjected to forced vibration can be written as follows:

$$\mathbf{M}\ddot{\mathbf{U}} + \mathbf{C}\dot{\mathbf{U}} + \mathbf{K}\mathbf{U} = \mathbf{F} \tag{5}$$

where $\mathbf{U}$ = displacements and rotations of each degree of freedom as

$$\mathbf{U} = [u_f \quad \theta_f \quad u_s]^T \tag{6}$$

Time derivatives of $\mathbf{U}$ are indicated with dots over the vector. Terms $\mathbf{M}$, $\mathbf{C}$, and $\mathbf{K}$ = mass, damping, and stiffness matrices, respectively, and are expressed as (adapted from Crouse and McGuire 2001):

$$\mathbf{M} = \begin{pmatrix} m_f + m_s & m_f h_f + m_s h & m_s \\ m_f h_f + m_s h & I_f + m_f h_f^2 + m_s h^2 & m_s h \\ m_s & m_s h & m_s \end{pmatrix} \tag{7a}$$

$$\mathbf{K} = \begin{pmatrix} k_x & k_{yx} & 0 \\ k_{xy} & k_{yy} & 0 \\ 0 & 0 & k_s \end{pmatrix} \tag{7b}$$

$$\mathbf{C} = \begin{pmatrix} c_x & c_{yx} & 0 \\ c_{xy} & c_{yy} & 0 \\ 0 & 0 & c_s \end{pmatrix} \tag{7c}$$

The use of strain-invariant stiffness and damping terms assumes an elastic response. Also, horizontal excitation is assumed in the x direction, meaning that θ = rotation in the $x - z$ plane (rotational stiffness and damping terms carry the yy subscript). The mass, height, and moment of inertia terms in Eq. (7*a*) are defined in Fig. 5; the diagonal foundation stiffness and damping terms in Eqs. (7*b*) and (7*c*) are defined in Eqs. (2), (3*a*), and (3*b*); the off-diagonal foundation stiffness and damping terms (k_{yx}, c_{yx}) in Eqs. (7*b*) and (7*c*) = coupling terms in the impedance function and are often approximated as zero for surface foundations; and the structural stiffness and viscous damping = k_s and c_s, respectively. Finally, $\mathbf{F}$ = a force vector expressed as (Crouse et al. 1984):

$$\mathbf{F} = [F_s \quad hF_s \quad F_s]^T \tag{8}$$

Equations of motion at each degree of freedom are obtained by entering the terms from Eqs. (6)–(8) into Eq. (5) and completing the

Table 1. Fixed and Flexible-Base Fundamental Mode Frequencies for the GVDA Model Test Structure

Excitation source	Structural configuration	Fixed-base parameters		Flexible-base parameters	
		f(Hz)	ζ (%)	f(Hz)	ζ (%)
Earthquake $M_L = 4.2$	Unbraced	6.70	0.51	5.82	1.25
Earthquake $M_w = 5.4$	Unbraced	6.70	0.90	5.81	4.11
Forced	Unbraced	6.56	1.48	6.04	1.68
Forced	Braced	12.76	9.33	9.88	4.60

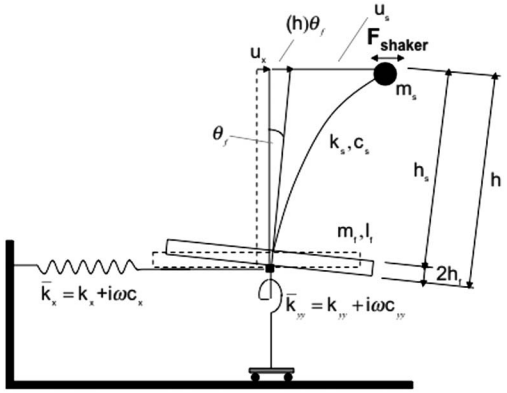

Fig. 5. Model for soil, foundation, and single-degree-of-freedom structure used to derive impedance functions

matrix multiplication. Excluding the coupled foundation stiffness and damping terms, the resulting equations are

$$\text{Foundation translation: } m_s(\ddot{u}_f + h\ddot{\theta}_f + \ddot{u}_s) + m_f(\ddot{u}_f + h_f\ddot{\theta}_f) + c_x\dot{u}_f + k_x u_f = F_s \tag{9}$$

$$\text{Foundation rotation: } m_s h(\ddot{u}_f + h\ddot{\theta}_f + \ddot{u}_s) + I_f\ddot{\theta}_f + m_f h_f(\ddot{u}_f + h_f\ddot{\theta}_f) + c_{yy}\dot{\theta}_f + k_{yy}\theta_f = hF_s \tag{10}$$

$$\text{Structure translation: } m_s(\ddot{u}_f + h\ddot{\theta}_f + \ddot{u}_s) + c_s\dot{u}_s + k_s u_s = F_s \tag{11}$$

In Eqs. (9)–(11), quantity $(\ddot{u}_f + h\ddot{\theta}_f + \ddot{u}_s)$ = measured roof acceleration; $\ddot{\theta}_f$ is calculated from vertical sensors on the foundation (difference of vertical accelerations divided by horizontal separation distance); and the top-of-foundation acceleration = $(\ddot{u}_f + 2h_f\ddot{\theta}_f)$. Hence, all the motions listed in Eqs. (9)–(11) are evaluated from the instrumentation depicted in Fig. 4. Applying Fourier transforms and writing Eqs. (9) and (10) in displacements yields:

$$-\omega^2 m_s(\bar{u}_f + h\bar{\theta}_f + \bar{u}_s) - \omega^2 m_f(\bar{u}_f + h_f\bar{\theta}_f) + i\omega c_x\bar{u}_f + k_x\bar{u}_f = \bar{F}_s \tag{12}$$

$$-\omega^2 m_s h(\bar{u}_f + h\bar{\theta}_f + \bar{u}_s) - \omega^2 I_f\bar{\theta}_f - \omega^2 m_f h_f(\bar{u}_f + h_f\bar{\theta}_f) + i\omega c_{yy}\bar{\theta}_f + k_{yy}\bar{\theta}_f = h\bar{F}_s \tag{13}$$

where the overbar indicates the variable in the frequency domain (obtained through Fourier transformation). Rearranging the previous equations yields the following:

$$-\omega^2 m_s(\bar{u}_f + h\bar{\theta}_f + \bar{u}_s) - \omega^2 m_f(\bar{u}_f + h_f\bar{\theta}_f) + (\bar{k}_x)\bar{u}_f = \bar{F}_s \tag{14}$$

$$-\omega^2 m_s h(\bar{u}_f + h\bar{\theta}_f + \bar{u}_s) - \omega^2 I_f\bar{\theta}_f - \omega^2 m_f h_f(\bar{u}_f + h_f\bar{\theta}_f) + (\bar{k}_{yy})\bar{\theta}_f = h\bar{F}_s \tag{15}$$

where the terms $\bar{k}_x$and $\bar{k}_{yy}$ = complex-valued translational and rotational foundation stiffnesses, respectively, as defined in Eq. (1*a*). Hence, the translational and rotational stiffness and damping can be evaluated in the frequency domain with the following equations:

$$\bar{k}_x = \frac{\bar{F}_s + \omega^2 m_s(\bar{u}_f + h\bar{\theta}_f + \bar{u}_s) + \omega^2 m_f(\bar{u}_f + h_f\bar{\theta}_f)}{\bar{u}_f} \tag{16}$$

$$\bar{k}_{yy} = \frac{h\bar{F}_s + \omega^2 m_s h(\bar{u}_f + h\bar{\theta}_f + \bar{u}_s) + \omega^2 I_f\bar{\theta}_f + \omega^2 m_f h_f(\bar{u}_f + h_f\bar{\theta}_f)}{\bar{\theta}_f} \tag{17}$$

Identical expressions for shaking in the y direction are obtained if the horizontal translations in Eqs. (16) and (17) are measured in the y direction and the foundation rotation is measured in the $y-z$ plane [denoted xx in Fig. 1(a)].

In Eq. (16), the complex translational stiffness term is equal to the ratio of the base shear to the foundation displacement. The complex rotational stiffness term in Eq. (17) is equal to the ratio of base moment to the foundation rotation. Through Eq. (1*a*), the real parts of these terms give the dynamic stiffness coefficient; the complex parts include the corresponding damping coefficient.

Eqs. (16) and (17) are validated by generating simulated data with a computational model of a structure similar to the one in Fig. 5 with a specified impedance function (including coupling terms). The normalized fundamental mode frequency for the system is $a_0 = 0.53$, which approximately matches the flexible-base frequency of the Garner Valley test structure. The data are generated by exciting the model with a broadband excitation force. Details of the forcing function are unimportant because the model of the structure-soil system is elastic. Computed data consisting of roof and foundation translational displacements and foundation rotation were then used to invert the foundation impedance with Eqs. (16) and (17). Fig. S1 shows the impedance ordinates used in the simulations and those returned by the inversion for this single-degree-of-freedom (SDOF) structure. Errors are small (less than 9%) and result from exclusion of the coupling impedance terms in the derivation of Eqs. (16) and (17). If coupling terms are excluded from the computational model producing the simulated data, then the match of impedance terms is essentially perfect.

A second set of simulations were performed for a two-degree-of-freedom structural system with intermediate-level mass of approximately 10% of the top mass. The system has an identical first-mode frequency to that considered previously ($a_0 = 0.53$) and a second-mode normalized frequency of $a_0 = 4.5$. Coupling impedance terms are not used in the simulations, so differences between assumed and inverted impedance ordinates result solely from higher mode effects. The inversion of foundation impedance is performed by using Eqs. (16) and (17), which neglects the inertia of the intermediate-level mass. The purpose of this simulation is to evaluate errors associated with the use of the SDOF inversion technique for a structure with a higher mode. As shown in Fig. S1, those results demonstrate no significant errors at low frequencies. However, errors occur at higher frequencies as the second mode is approached. This suggests that inverted impedance ordinates could be erroneous near higher mode frequencies.

Field Testing Program

Testing Overview

Two types of tests were carried out on the structure: fast sweep tests for the braced and unbraced configurations and harmonic tests for the braced configuration. In the fast sweep tests, the frequency of the shaker force was lowered gradually from 15 to 5 Hz in 60 s. In the harmonic tests, the frequency of the shaker force was held constant until the system reached steady state and for 30 cycles thereafter. The excitation frequency was then increased

by increments to the next level and the process was repeated. This type of test was also carried out in the frequency range of 5–15 Hz. The braced and unbraced experiments reported in this paper were both conducted on November 4, 2006, so that environmental conditions for the two tests were effectively identical.

Figs. 6(a) and 6(b) show Fourier amplitude spectra of the roof and base translation. The motions imposed during the tests are small—the peak displacement and acceleration of the roof are 0.005 cm and 0.009 g, respectively, and 0.0003 cm and 0.0006 g for the base. Accordingly, the structural and soil response were expected to remain in the elastic range. Also shown in Figs. 6(a) and 6(b) is the Fourier amplitude of noise from a horizontal instrument at the foundation level, which was recorded in a time interval with no external excitation. The roof translation is comfortably above the noise level across the full range of tested frequencies. The foundation translation approaches the noise level at approximately 14 and 9 Hz in the braced and unbraced structures, respectively. Fig. 6(c) shows Fourier spectra of rotation θ for tests on the braced and unbraced structure and for zero excitation (marked as "noise"). Like the translational motions, the braced signal is above the noise level for nearly the full range of frequencies, and the unbraced signal is closer to, but generally above, the noise level for frequencies below 10 Hz.

Analysis of Foundation Impedance from Test Data

Eqs. (16) and (17) are examples of transfer functions, which are ratios of time series in the frequency domain. Numerator terms represent base shear [Eq. (16)] and moment [Eq. (17)], which are derived from accelerations recorded in the time domain and then converted to the frequency domain by using the fast Fourier transformation (FFT). The FFT of a recorded acceleration is $-\omega^2\bar{u}$, in which $\bar{u}$ is the corresponding displacement. Denominators in Eqs. (16) and (17) are displacement and rotation terms obtained from the Fourier transformation of recorded acceleration divided by $-\omega^2$.

Fig. S2 in the electronic supplement plots loops of shear versus base displacement and moment versus base rotation for cycles of the braced structure at low frequencies (near 6 Hz), midfrequencies (near 10 Hz), and high frequencies (near 14 Hz). Similar plots for the unbraced structure are provided at 6, 7.5, and 9 Hz. Important features in these plots include (1) the secant moduli of the moment-rotation loops decrease markedly with frequency, indicating frequency dependence of the foundation rocking stiffness terms (k_{yy}), whereas the shear-sliding stiffnesses (k_x) are nearly independent of frequency; (2) the "fatness" of the loops is greater for shear-sliding than for moment-rotation, demonstrating the greater effectiveness of the shear-sliding deformation mode in foundation-soil energy dissipation; and (3) the loop fatness increases with frequency, demonstrating the contributions of radiation damping, which scales with frequency, to the overall foundation-soil damping.

The calculation of the transfer functions in Eqs. (16) and (17) is complicated by denominator terms that can be small at some frequencies owing to noise and other effects, causing the ratio to become very large. Accordingly, unsmoothed Fourier amplitude or phase spectra can have large frequency-to-frequency variability. Fig. 7(a) shows an example of unsmoothed transfer functions calculated by using Eq. (16); the result shown is the real part of the transfer function corresponding to the frequency-dependent foundation stiffness k_x, calculated by using signals recorded from the unbraced and braced structures excited in the fast sweep mode. Note the jagged appearance of the functions, which can complicate interpretation.

Mikami et al. (2008) review signal processing procedures (smoothing and windowing), which are designed to smooth transfer functions so that physically meaningful attributes are more readily discerned. Windowing involves the selection of the time segment considered in the analysis, which can be nontrivial for earthquake accelerograms. For the present application involving a controlled source, the time window is simply the untapered interval during which forced vibration is applied. Mikami et al. (2008) describe

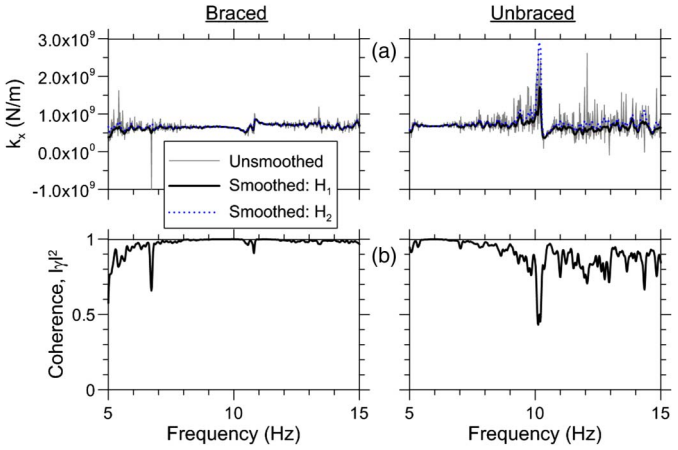

Fig. 7. (a) Example of smoothed and unsmoothed impedance results for translational foundation stiffness of braced and unbraced structures; (b) coherence of smoothed translational impedance estimates showing effects of noise

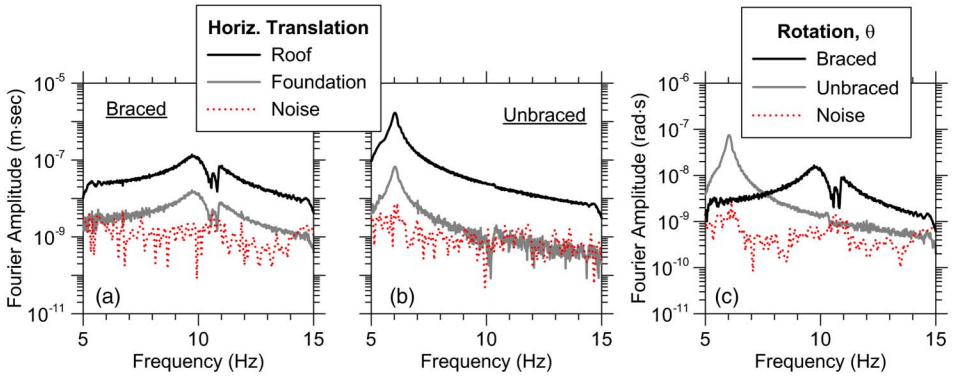

Fig. 6. (a) Fourier spectra of recorded horizontal displacements from fast sweep tests of braced structure; (b) same as (a), but for unbraced structure; (c) Fourier spectra of base rotations for braced and unbraced structure

time and frequency domain methods of smoothing and find little practical difference for a common level of smoothing as represented by an effective frequency bandwidth (a larger bandwidth implies greater smoothing). We employ frequency domain smoothing of power spectral density functions. Consider an arbitrary time series $a(t)$ sampled at N_t time steps having Fourier transform $\bar{a}(\omega)$. The smoothed autopower spectral density function is calculated as (Abrahamson 1992):

$$S_{aa}(\omega) = \sum_{j=-n}^{n} p_j \bar{a}(\omega_j)\bar{a}(\omega_j)^* \tag{18}$$

where $2n+1$ = number of discrete frequencies smoothed; $\omega_j = \omega + 2\pi j/N_t$; p_j = weights used in the frequency smoothing; and the asterisk denotes the complex conjugate. Smoothing is applied with an 11-point Hamming window ($n = 5$), which provides an effective frequency bandwidth of 0.13 Hz for the 60-s duration signals used to calculate the Fourier transforms (Mikami et al. 2008; Abrahamson 1992). A similar autopower spectral density function can be derived for time series $b(t)$. The complex-valued cross power spectral density function is calculated as

$$S_{ab}(\omega) = \sum_{j=-n}^{n} p_j \bar{a}(\omega_j)\bar{b}(\omega_j)^* \tag{19}$$

Two estimates of complex-valued transfer functions [e.g., the quantities in Eqs. (16) and (17)] are possible from these power spectral density functions (Pandit 1991):

$$H_1(\omega) = S_{ab}(\omega)/S_{aa}(\omega) \tag{20}$$

$$H_2(\omega) = S_{bb}(\omega)/S_{ba}(\omega) \tag{21}$$

The H_1 and H_2 estimates of the transfer function diverge in the presence of noise. Along with the unsmoothed transfer function described previously, Fig. 7(a) also shows the smoothed $H_1(\omega)$ and $H_2(\omega)$ estimates of the foundation stiffness k_x. The smoothed functions follow the same trend as the unsmoothed function but have a less jagged appearance.

Another valuable attribute of smoothing is that it allows the computation of coherence, which is the ratio of the two transfer function estimates (Pandit 1991):

$$\gamma^2(\omega) = \frac{H_1(\omega)}{H_2(\omega)} = \frac{|S_{ab}(\omega)|^2}{S_{aa}(\omega)S_{bb}(\omega)} \tag{22}$$

Coherence is theoretically unity in the absence of noise and drops below 1 for noisy signals, and hence, is useful for identifying the usable frequency range of a computed transfer function. Coherence values associated with the previous estimates of k_x are shown in Fig. 7(b). A comparison of the coherence function to the signal amplitudes from Figs. 6(a) and 6(b) shows that when coherence is low, it is because the amplitude of the denominator signal in Eq. (16) is approaching that of noise (i.e., signals recorded with no forced vibration). Transfer function ordinates associated with coherence < 0.8 were considered unreliable in some past work involving seismic signals (Kim and Stewart 2003; Mikami et al. 2008), although that threshold is somewhat arbitrary.

Considering both the coherence and noise spectra, the translational impedance estimates for the unbraced structure may not be reliable for frequencies higher than approximately 9 Hz. For the braced structure, the translational impedance should be reliable for frequencies higher than 5.5 Hz owing to high coherence and signals well above noise because of strong SSI. Similar interpretations of the rotational impedance terms are described subsequently.

Fig. 8 shows foundation impedance ordinates for translation and rocking calculated by using Eqs. (16) and (17) with transfer function estimate H_1 [Eq. (20)]. The stiffness ordinates (k_x, k_{yy}) represent the real part of the complex-valued stiffness, whereas the viscous dashpots (c_x, c_{yy}) are calculated from the imaginary part [through Eq. (1*a*)]. Three sets of results are shown for each stiffness and dashpot coefficient. Two are smoothed impedance ordinates calculated from time signals recorded with the braced and unbraced structure configurations. The third set of results is from harmonic tests, which were performed for the braced structure only. Those results are shown at discrete frequencies and are calculated directly from Eqs. (16) and (17) without the need for Fourier transformation or smoothing (the displacements and rotations are taken directly from the measured steady-state response). Results similar to those in this paper were obtained from multiple tests at various times.

Calculated impedance ordinates from the braced structure are consistent for the fast sweep and harmonic tests. Coherence values are high over the 5.5–15 Hz frequency range, suggesting minimal noise effects on the results.

Stiffness and damping for the unbraced structure are generally similar to those for the braced structure, but have more frequency-to-frequency variability as a result of reduced resolution of the foundation displacement and rotation signals. As previously stated, translational impedance ordinates for the unbraced structure are considered unreliable for frequencies greater than 9 Hz owing to excessive noise. The rotational results are considered reliable below 14 Hz because of high coherence and foundation rotations generally above the noise level. Interestingly, the unbraced rotational stiffness is less than the braced rotational stiffness by approximately 10% for frequencies under 8 Hz. This difference falls within the experimental error implicit to this method of field testing.

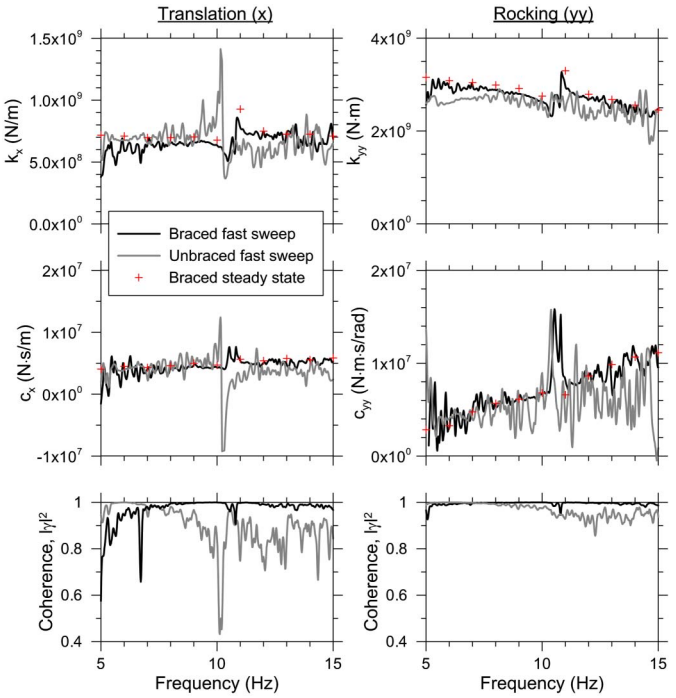

Fig. 8. Experimental foundation stiffness and damping values for horizontal translation and rocking obtained from testing of the Garner Valley test structure with and without bracing; and coherence estimates for the impedance ordinates

Impedance from Theoretical Solutions

Two principal aspects of theoretical models for foundation stiffness can be checked against the experimental data, the low-frequency (nearly static) stiffness and the variation of stiffness with frequency. Fig. 1(b) demonstrates that the variation of foundation stiffness with normalized frequency is similar for footings on a half-space and a depth-variable stiffness profile. Hence, because details of the soil layering are apparently of second-order importance, the critical question in the development of a theoretical prediction for comparison with the test results is the appropriate half-space shear wave velocity for calculations of static stiffnesses for horizontal translation and rocking. In most applications, V_s profiles are evaluated away from foundations (i.e., in the free-field) and show increases of stiffness with depth. To evaluate a single effective V_s value for use in computations, the user must (1) correct free-field V_s values to account for the increased overburden pressures associated with structure weight; and (2) select an appropriate depth range to average overburden-corrected velocities. The first effect is not considered in typical practice [e.g., there are no provisions for this in BSSC (2009)], but it was recognized by Dobry et al. (1986) and Gazetas and Stokoe (1991), who matched theoretical system frequencies to test data by using half-space velocities higher than free-field measured values. The second effect is considered in practice, as described subsequently.

Overburden corrections are not needed for the present application because the SASW results in Fig. 3 are based on arrays immediately adjacent to the foundation; hence, the measured velocities account for confinement provided by the structure weight. For more general applications in which velocities are measured in the free-field, we describe the process by which the overburden effect can be included in the analysis. Small-strain shear modulus (G) is known to increase with mean effective confining stress (σ'_m) as follows:

$$G = G_1 \left(\frac{\sigma'_m}{p_a} \right)^n \tag{23}$$

where G_1 = shear modulus for $\sigma'_m = 101.3$ kPa and n varies from approximately 0.5 for granular soils (Hardin and Black 1968; Marcuson and Wahls 1972) to 1.0 for cohesive soils with plasticity index PI $> \sim$6.5 (Yamada et al. 2008). Recognizing that V_s is proportional to the square root of shear modulus, free-field measurements of shear wave velocity are corrected to account for overburden effects from the structure as follows:

$$V_s \approx V_{s0} \left(\frac{\sigma'_{v0} + \Delta\sigma_v}{\sigma'_{v0}} \right)^{n/2} \tag{24}$$

where V_s = overburden-corrected shear wave velocity for a particular depth z; V_{s0} = shear wave velocity measured in the free-field; σ'_{v0} = effective stress from soil self weight at depth z; and $\Delta\sigma_v$ = increment of vertical stress at depth z from the structural weight, which can be computed by using classical stress distribution theory (e.g., Fadum 1948). The overburden correction in Eq. (24) is typically significant only at shallow depths below the foundation bearing level (approximately 50–100% of the foundation dimension).

Stewart et al. (2003) investigated the depth interval across which to compute an effective average profile velocity by matching half-space static stiffnesses to those of nonuniform profiles computed with the solutions of Wong and Luco (1985). The resulting recommendations, which are also given in BSSC (2009), compute effective profile velocity as the ratio of depth interval (z_p) to shear wave travel time through the depth interval, with the depth interval taken from the base of the footing to the following depths:

$$\text{Horizontal translation: } z_p = 0.75\sqrt{A_f/\pi} \tag{25}$$

$$\text{Rocking: } z_p = 0.75\sqrt[4]{4I_f/\pi} \tag{26}$$

where A_f = foundation area; and I_f = foundation moment of inertia. For the present structure, $Z_p = 1.7$ m and is measured from the ground surface because the foundation is not embedded. The V_s profile in Fig. 3 is depth-invariant in the upper 3 m, therefore, no averaging is needed and the profile velocity is assumed to be the values from the figure (the best estimate of $V_{sm} = 198$ m/s with a range of 183–213 m/s). Additional soil parameters used for the impedance calculation are mass density $\rho = 1{,}800$ kg/m^3 and Poisson's ratio $\nu = 0.35$. Small-strain soil damping ($D_{\min}$) is estimated at 2% from the empirical model of Darendeli (2001).

By using the previous soil parameters, impedance ordinates were calculated for horizontal translation and rocking using equations provided by Pais and Kausel (1988), which apply for a uniform half-space soil medium and rigid foundation. These model predictions are compared with experimental results in Fig. 9. The normalization of horizontal and rocking impedance in Fig. 9 is by G_mB and G_mB^3, respectively, where $G_m = \rho V_{sm}^2$; $B = 2m$ (foundation half-width); and $V_{sm} = 198$ m/s. Predictions calculated for the limits of the velocity range (183 and 213 m/s) are normalized with G_m to show the effect of velocity uncertainty. Frequency is normalized to a_0 [Eq. (4)], by using the velocity appropriate to each prediction [V_{sm} is used in Eq. (4) for experimental data]. In Fig. 9, experimental results are shown in the frequency range over which they are judged to be reliable on the basis of high coherence and minimal influence of noise, as described previously.

Considering first the stiffness results, predictions utilizing the best estimate velocity overestimate the experimental results by approximately 10% for translation and 15% for rotation. Predictions made with the reduced velocity (lower end of the range from Fig. 3) are consistent with experimental results. The stiffness decay

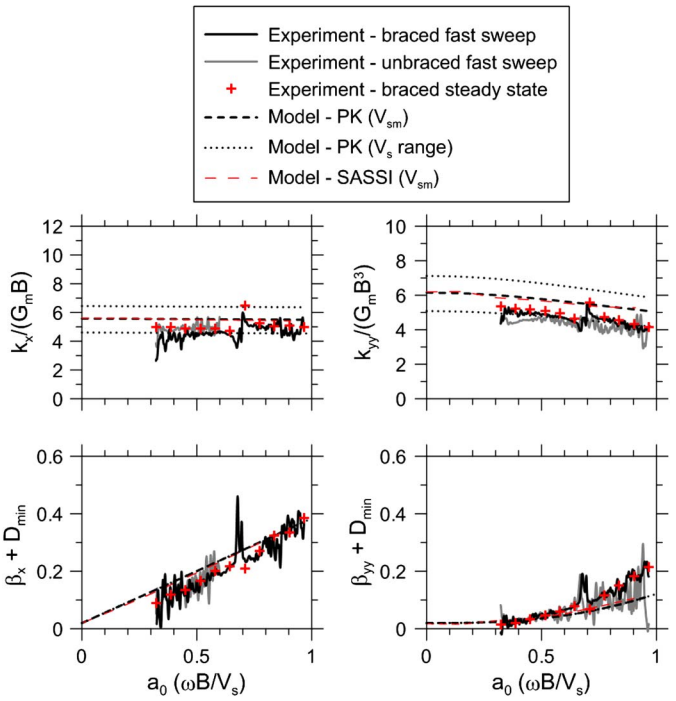

Fig. 9. Normalized impedance values from data compared with theoretical predictions for the Garner Valley site

with frequency is consistent between experimental results and predictions.

The normalized damping results (β_j terms) plotted in Fig. 9 represent half the ratio of the complex to the real part of the foundation impedance [Eq. (2)]. The results demonstrate finite damping at low frequencies that is slightly smaller than the model predictions. This suggests that the small-strain damping estimate of $D_{\min} = 2\%$ from Darendeli (2001) may be too large. Both the translational and rotational damping ordinates increase with frequency, which demonstrates the importance of radiation damping. Fig. 9 shows that $\beta_x > \beta_{yy}$, which confirms model predictions that radiation damping of square foundations in translation is a more significant energy dissipation mechanism than radiation damping in rotation. However, the model predictions for radiation damping are too high relative to data for translation and slightly too low for rotation.

Additional impedance estimates were computed by A. Mikami (personal communication, 2010) with the computer program SASSI (Ostadan 2006) with a finite concrete modulus (taken as 22 GPa) and a uniform half-space ($V_s = 198$ m/s). In the SASSI analysis, the first six soil layers are 0.25 m thick, followed by a 0.5-m layer and then 1.0-m layers extending to a half-space at 7 m of depth. Foundation loading was applied at the four corners of the 4-m-square foundation. Because the foundation is flexible in the SASSI analysis, the foundation displacements (and hence, the impedance) are location-dependent. Vertical displacements were taken from the corners (where the loads are applied) and horizontal displacements from the center of the foundation, which match the sensor locations used to calculate the experimental impedance (as shown in Fig. 4). Fig. 9 demonstrates that results from the two numerical models are nearly identical, indicating that the assumption of foundation rigidity in the Pais and Kausel (1988) model is reasonable for the present application.

Discussion and Conclusions

We present procedures to compute foundation stiffness and damping (impedance coefficients) for horizontal translational and rotational modes of foundation vibration from data recovered from forced vibration tests conducted on a soil-foundation-structure system. Implementation of the procedures requires measurements of horizontal motions at the roof and foundation level of the structure, vertical foundation motions to derive rotations, shaker forces, and system masses. The procedures are applied to data from the large-scale NEES SFSI field test structure in Garner Valley, California, that was subjected to fast sweep and harmonic excitation over a frequency range of 5–15 Hz. Applied force levels were small, so the structure-soil system was expected to have remained in the elastic range. The structure was tested both with and without bracing. The addition of bracing significantly increases the stiffness of the system and the importance of SFSI in the system response.

The identified impedance ordinates are frequency-dependent and complex-valued with real parts representing stiffness and complex parts damping. The stiffness terms demonstrate the decay of rotational stiffness with frequency and a relative lack of decay for translational stiffness. The damping terms show more pronounced energy dissipation for translational than rotational vibration modes, and increases of damping with frequency illustrate the importance of radiation damping for this foundation-soil system. Many of these features were previously anticipated in theoretical models but are now observed experimentally. The experimental impedance ordinates are in reasonable accord with predictions of theoretical models in which the soil medium is represented by a half-space, provided that consideration is given to the effects of structural weight on the soils' shear modulus and small-strain soil hysteretic damping. Stiffness terms are best matched by using a velocity slightly lower than the median from on-site measurements. Damping terms are modestly overpredicted for translation and underpredicted for rotation.

Acknowledgments

This work was partially supported by the Center for Embedded Network Sensing (CENS) at UCLA and also by fellowship funding from UCLA. This research made use of the testing facilities of NEES and NEES at UCSB. NEES Site PI Dr. Jamison Steidl is thanked for his assistance with site operation and data collection, as are NEES at UCSB staff Hank Ratzesberger and Paul Hegarty. We thank Timothy Ancheta, Dennis Hiltunen, George Mylonakis, and Dimitris Pitilakis for helpful discussions over the course of this research. We thank Lisa Star for independently checking the test results. Two anonymous reviewers are thanked for their helpful comments. We thank Dr. Atsushi Mikami for performing the SASSI runs for the test structure.

References

Abrahamson, N. A. (1992). "Spatial variation of earthquake ground motion for application to soil–structure interaction." *Rep. No. TR-100463*, Electrical Power Research Institute, Palo Alto, CA.

ASCE. (2006). "Seismic rehabilitation of existing buildings." *ASCE/SEI 41-06*, Reston, VA.

Andrus, R. D., Stokoe, K. H., II, and Juang, C. H. (2004). "Guide for shear-wave-based liquefaction potential evaluation." *Earthquake Spectra*, 20(2), 285–308.

Apsel, R. J., and Luco, J. E. (1987). "Impedance functions for foundations embedded in a layered medium: An integral equation approach." *Earthquake Eng. Struct. Dyn.*, 15(2), 213–231.

Building Seismic Safety Council (BSSC). (2009). "NEHRP recommended seismic provisions for new buildings and other structures." *Rep. FEMA P-750*, FEMA, Washington DC.

Clough, R. W., and Penzien, J. (1993). *Dynamics of structures*, McGraw Hill, New York.

Crouse, C. B., Hushmand, B., Luco, J. E., and Wong, H. L. (1990). "Foundation impedance functions: Theory versus experiment." *J. Geotech. Eng.*, 116(3), 432–449.

Crouse, C. B., Liang, G. C., and Martin, G. R. (1984). "Experimental study of soil-structure interaction at an accelerograph station." *Bull. Seismol. Soc. Am.*, 74(5), 1995–2013.

Crouse, C. B., and McGuire, J. (2001). "Energy dissipation in soil-structure interaction." *Earthquake Spectra*, 17(2), 235–259.

Darendeli, M. (2001). "Development of a new family of normalized modulus reduction and material damping curves." Ph.D. dissertation, Dept. of Civil, Architectural, and Environmental Engineering Univ. of Texas, Austin, TX.

de Barros, C. P., and Luco, J. E. (1995). "Identification of foundation impedance functions and soil properties from vibration tests of the Hualien containment model." *Soil Dyn. Earthquake Eng.*, 14(4), 229–248.

Dobry, R., Gazetas, G., and Stokoe, K. H., II. (1986). "Dynamic response of arbitrarily shaped foundations: Experimental verification." *J. Geotech. Eng.*, 112(2), 136–154.

Fadum, R. E. (1948). "Influence values for estimating stresses in elastic foundations." *Proc. 2nd Int. Conf. Soil Mechanics and Foundation Engineering*, Rotterdam, Vol. 3, 77–84.

Gadre, A., and Dobry, R. (1998). "Lateral cyclic loading centrifuge tests on square embedded footing." *J. Geotech. Geoenviron. Eng.*, 124(11), 1128–1138.

Gajan, S., and Kutter, B. L. (2008). "Capacity, settlement, and energy dissipation of shallow footings subjected to rocking." *J. Geotech. Geoenviron. Eng.*, 134(8), 1129–1141.

Gazetas, G. (1991). "Formulas and charts for impedances of surface and embedded foundations." *J. Geotech. Eng.*, 117(9), 1363–1381.
Gazetas, G., and Stokoe, K. H., II. (1991). "Free vibration of embedded foundations: Theory versus experiment." *J. Geotech. Eng.*, 117(9), 1382–1401.
Hardin, B. O., and Black, W. L. (1968). "Vibration modulus of normally consolidated clay." *J. Soil Mech. Found. Div.*, 94(2), 353–369.
Iguchi, M., and Luco, J. E. (1982). "Vibration of flexible plate on viscoelastic medium." *J. Eng. Mech.*, 108(6), 1103–1120.
Kim, S., and Stewart, J. P. (2003). "Kinematic soil-structure interaction from strong motion recordings." *J. Geotech. Geoenviron. Eng.*, 129(4), 323–335.
Lin, A. N., and Jennings, P. C. (1984). "Effect of embedment on foundation-soil impedances." *J. Eng. Mech.*, 110(7), 1060–1075.
Luco, J. E, Trifunac, M. D., and Wong, H. L. (1988). "Isolation of soil structure interaction effects by full-scale forced vibration tests." *Earthquake Eng. Struct. Dyn.*, 16(1), 1–21.
Marcuson, W. F., and Wahls, H. E. (1972). "Time effects on dynamic shear modulus of clays." *J. Soil Mech. Found. Div.*, 98(12), 1359–1373.
Mikami, A., Stewart, J. P., and Kamiyama, M. (2008). "Effects of time series analysis protocols on transfer functions calculated from earthquake accelerograms." *Soil Dyn. Earthquake Eng.*, 28(9), 695–706.
Nii, Y. (1987). "Experimental half-space dynamic stiffness." *J. Geotech. Eng.*, 113(11), 1359–1373.
Novak, M. (1987). "Discussion of 'Dynamic response of arbitrarily shaped foundations: Experimental verification' by Ricardo Dobry, George Gazetas, and Kenneth H. Stokoe II." *J. Geotech. Eng.*, 113(11), 1410–1412.
Ostadan, F. (2006). *SASSI2000: A system for analysis of soil-structure interaction, Revision 2, user's manual*, Bechtel, San Francisco.
Pais, A., and Kausel, E. (1988). "Approximate formulas for dynamic stiffnesses of rigid foundations." *Soil Dyn. Earthquake Eng.*, 7(4), 213–227.
Pandit, S. M. (1991). *Modal and spectrum analysis*, Wiley, New York.
Richart, F. E., Jr., and Whitman, E. V. (1967). "Comparison of footing vibration tests with theory." *J. Soil Mech. and Found. Div.*, 93(6), 143–168.
Stewart, J. P., Kim, S., Bielak, J., Dobry, R., and Power, M. (2003). "Revisions to soil structure interaction procedures in NEHRP design provisions." *Earthquake Spectra*, 19(3), 677–696.
Stewart, J. P., Whang, D. H., Nigbor, R. L., Wallace, J. W., and Kim, S. (2005). "Role of field performance data in development and calibration of seismic soil-structure interaction analysis procedures." *Soil-Structure Interaction: Calculation Methods and Engineering Practice, Proc. of the Int. Geotechnical Conf. Dedicated to the Tercentenary of St. Petersburg*, V. M. Ulitsky, ed., Vol. 1, St. Petersburg, Russia, 47–58.
Stokoe, K. H., II, Kurtulus, A., and Menq, F.-H. (2004). "Data report-SASW measurements at the NEES Garner Valley Test Site, California." Dept. of Civil Engineering, Univ. of Texas, Austin, ⟨http://nees.ucsb.edu/⟩ (2010).
Tileylioglu, S. (2008). "Evaluation of soil-structure interaction effects from field performance data." Ph.D. dissertation, Dept. of Civil and Environmental Engineering, Univ. of California, Los Angeles.
Veletsos, A. S., and Wei, Y. T. (1971). "Lateral and rocking vibrations of footings." *J. Soil Mech. and Found. Div.*, 97(9), 1227–1248.
Vrettos, C. (1999). "Vertical and rocking impedances for rigid rectangular foundations on soils with bounded non-homogeneity." *Earthquake Eng. Struct. Dyn.*, 28(12), 1525–1540.
Wong, H. L., and Luco, J. E. (1985). "Tables of impedance functions for square foundations on layered media." *Soil Dyn. Earthquake Eng.*, 4(2), 64–81.
Wong, H. L., Trifunac, M. D., and Luco, J. E. (1988). "A comparison of soil-structure interaction calculations with results of full-scale forced vibration tests." *Soil Dyn. Earthquake Eng.*, 7(1), 22–31.
Yamada, S., Hyodo, M., Orense, R. P., Dinesh, S. V., and Hyodo, T. (2008). "Strain-dependent dynamic properties of remolded sand-clay mixtures." *J. Geotech. Geoenviron. Eng.*, 134(7), 972–981.
Youd, T. L., Steidl, J. H., and Nigbor, R. L. (2004). "Ground motion, pore water pressure and SFSI monitoring at NEES permanently instrumented field sites." *Proc. 11th Int. Conf. on Soil Dynamics and Earthquake Engineering and the 3rd Int. Conf. on Earthquake Geotechnical Enginering*, PEER, Vol. 2, 435–442.